OPEN ACCESS

1st International Electronic Conference on Remote Sensing
22 June - 5 July 2015

Conference Proceedings Paper – Remote Sensing

Investigating Urban Heat Island Estimation and Relation between Various Land Cover Indices in Tehran City Using Landsat 8 Imagery

Mahdi Hasanlou [1,*] and Nikrouz Mostofi [2,†]

[1] University of Tehran, College of Engineering, Faculty of Surveying and Geospatial Engineering., Tehran, Iran; E-Mail: hasanlou@ut.ac.ir

[2] Islamic Azad University, South Tehran Branch, Department of Surveying Engineering. Tehran, Iran; E-Mail: n_mostofi@ azad.ac.ir

† These authors contributed equally to this work.

* Corresponding author; E-Mail: hasanlou@ut.ac.ir;
Tel.: +98-21-6111-4525; Fax: +98-21-8800-8837.

Published: 25 June 2015

Abstract: Nowadays, global warming has become more interested for scientist, because the global surface temperature has been increased since last century. The urban heat island (UHI) refers to the event of higher atmospheric and surface temperatures occurring in cities than in the surrounding rural areas due to urbanization. This phenomena can affect societies by increasing summertime, air pollution, air conditioning costs, heat related illness, greenhouse gas emissions and water quality. In this paper Tehran city used as case study area. Due to rapid urbanization progress that has resulted in significant UHI effect in this area. In this study, new launched Landsat series (Landsat 8) was used for monitoring UHI and retrieving the brightness temperatures and land use/cover types. In order to monitor the relationship between UHI and land cover indices, this paper tried to employ a quantitative approach for exploring the relationship land surface temperature (LST) and common land cover indices (i.e. NDVI, EVI, SAVI, NDWI, NDBaI, NDBI, MNDWI, BI, UI, IBI and EBBI). In this regards, the objectives of this research are to develop a kernel base analysis model for urban thermal environment by employing Support Vector Regression (SVR) algorithm.

Keywords: Urban heat island; land use/cover indices; support vector regression.

---

1. Introduction

The surface temperature is key factor for studying of urban climatology. It modifies the air temperature of the lowest layers of the urban atmosphere and also helps to determine the internal weathers of buildings and affects the energy balances that affect the comfortable city life **[1]**. The urban heat island (UHI) refers to the event of higher atmospheric and surface temperatures occurring in cities than in the surrounding rural areas due to urbanization, particularly at night **[2]**. The annual average air temperature of urban area with almost one million people can be one to three degree warmer than its surroundings. This phenomena can affect societies by increasing summertime, air pollution, air conditioning costs, heat related illness, greenhouse gas emissions and water quality. More than fifty percent of people are living in cities **[3]**, in this regard, urbanization has become a key factor for global warming. Tehran, a capital city of Iran is case study of this research. Additionally, Tehran is one of megacities of the world. A megacity is usually defined as a metropolitan area with a total population in excess of ten million people **[4]**. Due to rapid urbanization progress that has resulted in significant UHI effect in this area. Furthermore, Tehran houses to almost twenty percent of Iranian people. Normally, UHIs have been monitored by in situ observations taken from thermometer networks. Recently, by incorporating thermal remote sensing technology, remote observation of UHIs has become available using satellite imageries and has facilitated monitoring of UHI. Satellite thermal imageries, especially high resolution imagery, has the advantage of providing a repeatable dense grid of temperature data over a whole city and even distinctive temperatures for individual buildings.

Previous investigations of land surface temperatures (LST) and thermal remote sensing of urban areas have been conducted primarily by using AVHRR or MODIS imageries **[5,6]**. Currently, researchers all around the world use high resolution satellite imagery for investigating about thermal anomalies in urban area **[7–9]**. In this study, new launched Landsat series (Landsat 8) was used for monitoring UHI and retrieving the brightness temperatures and land use/cover types. The Landsat 8 carries two kind of sensors **[10]**: The Operational Land Imager (OLI) sensor has former Landsat bands, with three new bands: a deep blue band for coastal/aerosol studies (band 1), a shortwave infrared band for cirrus detection (band 9), and a Quality Assessment band. The Thermal Infrared Sensor (TIRS) sensor provides two high resolution (near to 30 meters) thermal bands (band 10, 11). These sensors both use corrected signal-to-noise (SNR) radiometric quantized over a 12-bit. Corrected SNR performance cause better determination of land cover type. Moreover, Landsat 8 images incorporate two valuable thermal bands in 10.9 µm and 12.0 µm. These two thermal bands improve estimation of UHI by incorporating split-window methods and has also increased opportunities for studying the UHI and urban-modified climates more generally.

The UHIs can be affected by three main factors **[7]**: 1) the effects of energy transformation in urban area; 2) reduced evapotranspiration; and (3) anthropogenic energy production. Also, according **[11]**, there are three types of UHIs: 1) Canopy Layer Heat Island (CLHI); 2) Boundary Layer Heat Island (BLHI); and 3) Surface Heat Island (SHI). The difference between these types of UHI are described by **[9]**. The main characterizing of CLHI and is that BLHI represent as warming the urban atmosphere and SHI represent as warming the urban surface. Also, the main difference between CLHI and SHI is place

where temperature is appeared and detected. Usually, CLHI is detected by fixed air temperature measurement (in situ data) in the canopy layer, while remotely sensed thermal imageries observe the spatial patterns of upwelling thermal radiance to estimate the LST **[1]** of the SHI.

Recently, quantitative models for urban thermal environment and related factors have been studied, for example, the relation between UHI and land cover structure and established corresponding regression equation **[2,8]**. Similar works have been done and models of the relation between the surface temperature and various vegetation indices have been established **[12,13]**. In order to monitor the relationship between UHI and land cover indices, this paper tried to employ a quantitative approach for exploring the relationship SHI and common land cover indices and select suitable indices, including the Normalized Difference Vegetation Index (NDVI) **[14]**, Enhanced Vegetation Index (EVI) **[14]**, Soil Adjusted Vegetation Index (SAVI) **[15]**, Normalized Difference Water Index (NDWI) **[16]**, Normalized Difference Bareness Index (NDBaI) **[13,17]**, Normalized Difference Build-up Index (NDBI) **[18]**, Modified Normalized Difference Water Index (MNDWI) **[19]**, Bare Soil Index (BI) **[17,18]**, Urban Index (UI) **[20]**, Index-based Built-Up Index (IBI) **[21]** and Enhanced Built-Up and Bareness Index (EBBI) **[22]**. Behind these indices, the tasselled cap transformation (TCT) that calculated for Landsat 8 imagery is used for compressing spectral data into a few bands associated with physical scene characteristics with minimal information loss **[23]**. The three TCT information, Brightness, Greenness and Wetness computed and incorporated for predication of UHI effect. In this regards, the objectives of this research are to develop a non-linear and kernel base analysis model for urban thermal environment by employing Support Vector Regression (SVR) method **[24]**.

2. Proposed Method

In this study Landsat 8 imagery was used as input data for estimation SHI map and also various urban and vegetation indices. The **Figure 1**. illustrated the flowchart of proposed methods.

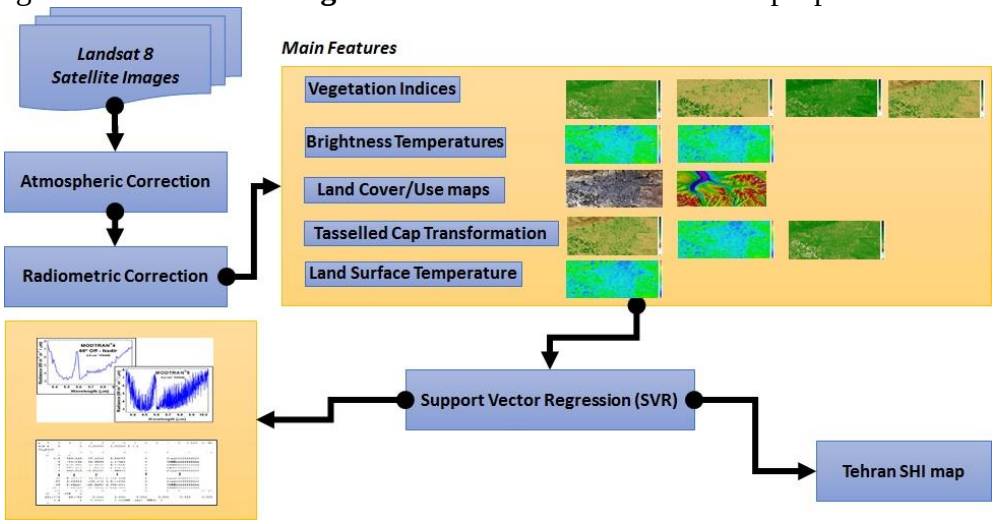

Figure 1. Flowchart of proposed methods.

As it clear form **Figure 1.**, after importing Landsat 8 imagers, atmospheric and radiometric correction is done. The next step starts with producing urban and vegetation indices with brightness temperature (BT) of thermal bands in 10.9 µm and 12.0 µm (band 10, 11) [25]. In addition in this step

by incorporating Landsat 8 LST algorithm that introduced in [26], we calculate LST data for our datasets by using split-window (SW) algorithm (Eq 1.).

$$LST = c_0 + T_{b10} + c_1(T_{b10} - T_{b11}) + c_1(T_{b10} - T_{b11})^2 + (c_3 + c_4\omega)(1 - \varepsilon) + (c_5 + c_6\omega)\Delta\varepsilon \quad (1)$$

where T_{b10} and T_{b11} are the at sensor BTs (in kelvins), ε is the mean emissivity, $\varepsilon = 0.5(\varepsilon_{b10} + \varepsilon_{b11})$, $\Delta\varepsilon$ is the emissivity difference, $\Delta\varepsilon = (\varepsilon_{b10} - \varepsilon_{b11})$, ω is the total atmospheric water vapor content (in $g \cdot cm^{-2}$) that we set to $\omega = 3$ as mention in [26], and c_0 to c_6 are the SW coefficients that computed in [26]. For estimating ε_{b10} and ε_{b11} in this study, we incorporate simultaneously MODIS product [27] for same area. In the next section procedure of computing urban and vegetation indices are introduced.

2.1. Urban and Vegetation Indices

The main and most important urban and vegetation indices are used in this study. These indices can be divided to two type: 1) urban indices and 2) vegetation indices.

2.1.1. Urban Indices

The widespread and common urban indices are shown in the Table 1. The most of these indices extract urbanization parameters related to spectral difference of visible, near infrared and short wave infrared bands of Landsat 8 Imagery. All indices from Table 1. calculated based on incorporating digital number (DN) of Landsat 8 bands.

Table 1. Extracted urban indices form Landsat 8 imagery.

No.	Name of urban index	Formulation
1	Normalized Difference Bareness Index (NDBaI)	$NDBaI = \frac{SWIR1 - TIRS1}{SWIR1 + TIRS1}$
2	Normalized Difference Build-up Index (NDBI)	$NDBI = \frac{SWIR1 - NIR}{SWIR1 + NIR}$
3	Bare Soil Index (BI)	$BI = \frac{(SWIR1 + RED) - (NIR + BLUE)}{(SWIR1 + RED) + (NIR + BLUE)}$
4	Urban Index (UI)	$UI = \frac{SWIR2 - NIR}{SWIR2 + NIR}$
5	Index-based Built-Up Index (IBI)	$IBI = \frac{\frac{2\times SWIR1}{SWIR1+NIR} - (\frac{NIR}{NIR+RED} - \frac{GREEN}{GREEN+SWIR1})}{\frac{2\times SWIR1}{SWIR1+NIR} + (\frac{NIR}{NIR+RED} - \frac{GREEN}{GREEN+SWIR1})}$
6	Enhanced Built-Up and Bareness Index (EBBI)	$EBBI = \frac{SWIR1 - NIR}{10\sqrt{SWIR1 + TIRS1}}$

2.1.2. Vegetation Indices

As before, in the Table 2. computable vegetation indices extracted from spectral bands like, visible, near infrared and short wave infrared bands of Landsat 8 Imagery are illustrated. All these indices calculated based on incorporating radiance (Rad) or reflectance (Ref) of related Landsat 8 bands by using procedure introduced in [25].

Table 2. Extracted vegetation indices form Landsat 8 imagery.

No.	Name of urban index	Formulation
1	Normalized Difference Vegetation Index (NDVI)	$NDVI = \frac{NIR - RED}{NIR + RED}$
2	Enhanced Vegetation Index (EVI)	$EVI = G \times \frac{NIR - RED}{NIR + C_1 \times RED - C_2 \times BLUE + L}$ $L = 1;\ C_1 = 6;\ C_2 = 7.5; G = 2.5$
3	Soil Adjusted Vegetation Index (SAVI)	$SAVI = \frac{NIR - RED}{NIR + RED + L} \times (L + 1)$ $0 < L < 1 \Rightarrow L = 0.5$
4	Normalized Difference Water Index (NDWI)	$NDWI = \frac{NIR - SWIR1}{NIR - SWIR1}$
5	Modified Normalized Difference Water Index (MNDWI)	$MNDWI = \frac{GREEN - NIR}{GREEN + NIR}$
6	Tasselled Cap Transformation (TCT)	Brightness
7	Tasselled Cap Transformation (TCT)	Greenness
8	Tasselled Cap Transformation (TCT)	Wetness

2.2 Support Vector Regression

The SVR is a new supervised learning method which emerged in late 1970s [24]. SVR allows computing a powerful nonparametric approximation of the relationship between urban/vegetation indices and SHI change. This technique is also used in most remote sensing applications like LST and SST retrieval [28], biophysical parameter estimation and other leaf area index estimation from multispectral satellite images [29].

Consider a set of training points, $\{(x_1, z_1), \dots, (x_l, z_l)\}$, where $x_i \in \mathbb{R}^n$ is a feature vector and $z_i \in \mathbb{R}^1$ is the target output. Under given parameters $C > 0$ and $\epsilon > 0$ the standard form of support vector regression [24,30] is

$$\begin{aligned} \min_{\omega, b\xi, \xi^*} \frac{1}{2}\omega^T\omega + C\sum_{i=1}^{l}(\xi_i + \xi_i^*) \\ \text{subject to } \omega^T\phi(x_i) + b - z_i \le \epsilon + \xi_i \\ z_i - \omega^T\phi(x_i) - b \le \epsilon + \xi_i^* \\ \xi_i, \xi_i^* \ge 0, i = 1, \dots, l \end{aligned} \tag{2}$$

By introducing Lagrange multipliers and exploiting the optimality constraints, the decision function has the following explicit form:

$$\sum_{i=1}^{l}(\alpha_i + \alpha_i^*)K(x_i, x) + b, \qquad 0 \le \alpha_i \le C, 0 \le \alpha_i^* \le C \tag{3}$$

where l is the number of support vectors (SVs) and the kernel function

$$K(x_i, x) = \sum_{j=1}^{m}\phi_j(x)\phi_j(x_i) \tag{4}$$

and α_i^* are Lagrange multipliers.

3. Experimental Result

In this study two Landsat 8 images that acquired from Tehran city area was used as datasets. Information about these images are represented in Table 3. Dataset #1 is belong to summer time that air temperature in these times is near to1 40^{o}C, and another one is belong to winter time.

Table 3. Landsat 8 images for studying SHI

Dataset	Acquisition date	Area
#1	15-JUN-14	Tehran City
#2	08-DEC-14	Tehran City

As mention in previous section by incorporating Landsat 8 LST retrieval algorithm (Eq. 1) and contemporary MODIS product for estimating emissivity of two thermal bands (i.e. ε_{b10} and ε_{b11}), SHI is estimated. In addition, urban, vegetation and TCT (Brightness, Greenness and Wetness) indices from DN/Ref Landsat 8 images were calculated. Calculated indices and information using dataset #1 is shown in **Figure 2**.

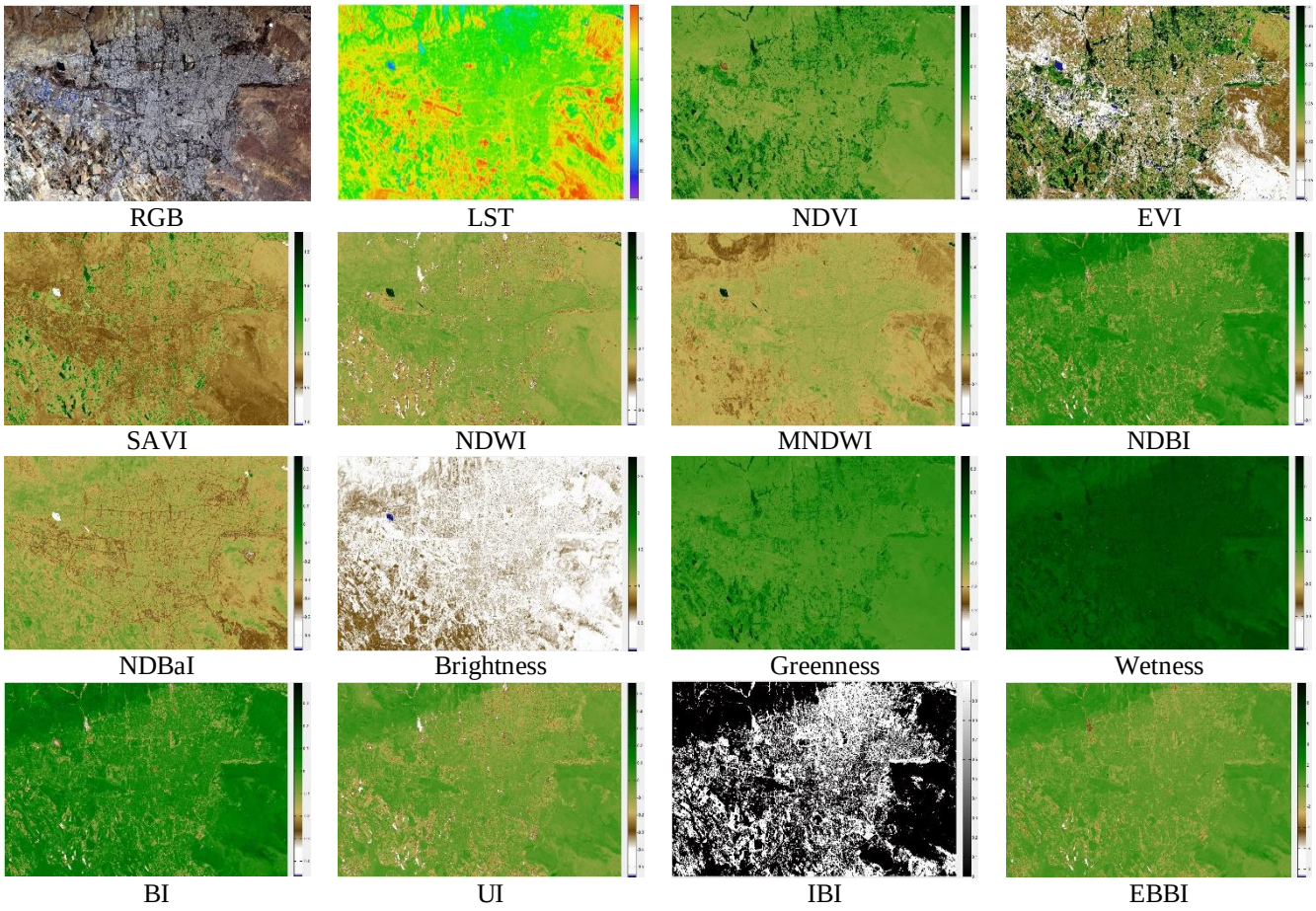

Figure 2. Urban, vegetation and TCT indices for dataset #1.

Same computation is done for dataset #2 and calculated urban, vegetation and TCT (Brightness, Greenness and Wetness) indices are illustrated in Figure 3.

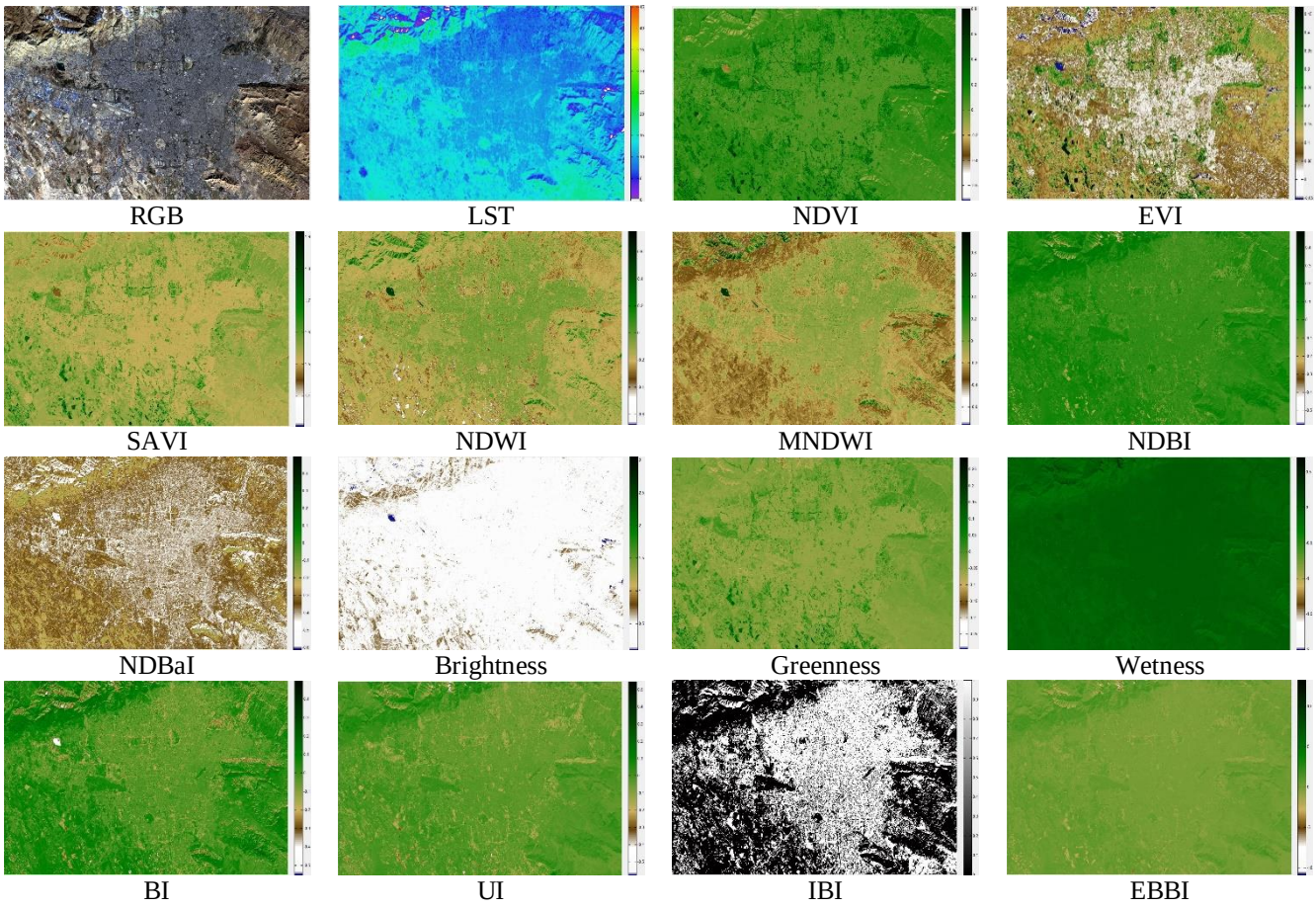

Figure 3. Urban, vegetation and TCT indices for dataset #2.

Next step is performed by SVR technique to relate extracted urban, vegetation and TCT indices to SHI data (Eq. 5).

$$SHI = f(NDVI, EVI, SAVI, NDWI, MNDWI, Brightness, Greenness, Wetness, NDBaI, NDBI, BI, UI, IBI, EBBI) \quad (5)$$

In this regards, as mention in previous section we adopted SVR technique. In SVR, the parameter C computes the tradeoff between the flatness and the degree to which deviations larger than ε are tolerated in the optimization formulation. In this manner, if C is too large, then the objective is to minimize the empirical risk without regard to flatness part in the optimization formulation. The bigger the ε is, the fewer support vectors will be included. Therefore, more 'flat' estimation is consequence of bigger ε values. In fact, both C and ε values affect the flatness (model complexity). In this paper, C value is computed by (Eq. 6) base on [31].

$$C = \max(Training\ data) - \min(Training\ data) \quad (6)$$

Also, a Gaussian radial basis function (RBF) kernel (Eq. 4) is used; this function is widely used in remote sensing algorithm. Prior to the estimating regression stage, simple scaling/normalizing must be done on the training data. The main advantage of scaling is to avoid attributes in greater numeric ranges dominating those in smaller numeric ranges. Another advantage is to reduce numerical

complexity during the computation. The next step is the training procedure, during which some critical SVR parameters ε and in the RBF kernel γ, must be specified. A simple tool to check a grid of parameters is provided by cross-validation (CV) error (i.e. mean square error (MSE)) with 5-fold. Range of grid search method for estimating ε parameter is [0,5] and for γ RBF parameter is $[2^{-7},2^{7}]$. Then, 720 (30% of data) random point was selected as training data and 1680 (70% of data) random point is selected as testing data extracted from dataset #1 and #2. In this manner, Table 4. and 5. are illustrated the optimum SVR parameters estimation for dataset #1 and #2 respectively. It is obvious from Table 4. that the optimum SVR parameters for dataset #1 are $\epsilon = 0, \gamma = 2$ and C=22.40. Again, from Table 5. the optimum SVR parameters for dataset #2 are $\epsilon = 0, \gamma = 1$ and C=15.14.

Table 4. Optimum SVR parameters estimation for dataset #1 with C= 22.4013.

	$\epsilon = 0$	1	2	3	4	5
$\gamma = 2^{-7}$	8.9248	8.9647	9.044	9.2615	9.4912	9.8826
2^{-6}	8.1931	8.302	8.4365	8.8251	9.0959	9.6601
2^{-5}	7.2267	7.3276	7.672	8.1622	8.5831	9.2708
2^{-4}	5.8522	5.9942	6.6195	7.2668	7.9778	8.76
2^{-3}	3.9949	4.4532	5.2895	6.2399	7.2854	8.105
2^{-2}	2.372	2.9398	3.9742	5.2427	6.397	7.4099
2^{-1}	1.5473	2.1104	3.174	4.4679	5.7297	6.8946
2^{0}	1.4013	1.801	2.8437	4.0502	5.4578	6.598
2^{1}	**1.3833**	1.6836	2.552	3.7709	5.1794	6.5787
2^{2}	1.5092	1.6205	2.4686	3.7119	5.2035	6.759
2^{3}	1.7264	1.8258	2.6858	3.9737	5.3606	7.1223
2^{4}	1.9631	2.2332	3.2883	4.468	5.9297	7.6059
2^{5}	2.4885	2.9571	4.2283	5.5619	6.9744	8.2201
2^{6}	3.554	4.1001	5.4872	6.8119	8.1602	9.2165
2^{7}	5.1897	5.94	7.131	8.2575	9.3713	10.3855

Table 5. Optimum SVR parameters estimation for dataset #2 with C= 15.1443.

	$\epsilon = 0$	1	2	3	4	5
$\gamma = 2^{-7}$	3.5728	3.6203	3.7465	3.9453	4.2763	4.9328
2^{-6}	3.2757	3.3461	3.5428	3.8146	4.1926	4.8525
2^{-5}	2.8064	2.9516	3.2566	3.6565	4.0248	4.6816
2^{-4}	2.1372	2.3853	2.873	3.4025	3.8541	4.633
2^{-3}	1.3728	1.7408	2.3534	3.1273	3.6953	4.4949
2^{-2}	0.8369	1.214	1.9527	2.8148	3.6012	4.3988
2^{-1}	0.6188	0.9288	1.6741	2.5687	3.51	4.3752
2^{0}	**0.552**	0.7768	1.495	2.4868	3.3917	4.4282
2^{1}	0.5736	0.7643	1.4816	2.4259	3.3971	4.624
2^{2}	0.6387	0.8361	1.5391	2.4159	3.5788	4.9251
2^{3}	0.7551	0.9701	1.7051	2.7299	3.7836	5.0233
2^{4}	0.9101	1.1954	2.0664	3.0564	4.0309	5.0652
2^{5}	1.2115	1.5772	2.4113	3.3655	4.1731	5.2
2^{6}	1.6435	2.0494	2.8103	3.6314	4.4022	5.3901
2^{7}	2.2376	2.6204	3.2666	3.9472	4.6724	5.6117

By incorporating the best estimated parameters (ϵ, γ and C) with minimum validation error (MSE), the performance of the selected final SVR model is computed for dataset #1 (Table .6) and dataset #2 (Table. 7) respectively.

Table 6. The performance of final SVR model for dataset #1.

	MSE	NRMS	R^2
Training	0.7507	0.2424	0.9442
Test	1.1155	0.3053	0.9100

As it clear from both Table 6. and Table 7. that, there are high degree of consistency between incorporated information for each dataset and SHI. For example, correlation coefficient between training and test data are R^2= 0.9442 and R^2=0.9100 for dataset #1. Also, correlation coefficient between training and test data are R^2= 0.9113 and R^2=0.9051 for dataset #2.

Table 7. The performance of final SVR model for dataset #2.

	MSE	NRMS	R^2
Training	0.4307	0.3035	0.9113
Test	0.4546	0.3113	0.9051

4. Conclusions

All range of Landsat 8 spectral bands have been used for estimating SHI of Tehran city, especially thermal bands. In this study, urban indices including NDBaI, NDBI, BI, UI, IBI and EBBI have been calculated using recent urban parameters and factors. In addition, for better investigating vegetation factors, more common vegetation and water indices including NDVI, EVI, SAVI, NDWI and MNDWI behind TCT information including Brightness, Greenness and Wetness have been used. By utilizing these information and indices modeling and monitoring of SHI are more feasible. Also as part of this study, the powerful regression model, the SVR is used to monitor SHI variation in two different time (dataset #1 and #2) from summer to winter. Incorporating this procedure reveled that there is high degree of consistency between affected information and LST images (MSE=0.75 for dataset #1 and MSE=0.43 for dataset #2). This study must be completed by incorporating supervised feature selection method to select suitable features and indices from urban and vegetation information.

References and Notes

1. Voogt, J. A.; Oke, T. R. Thermal remote sensing of urban climates. *Remote Sens. Environ.* **2003**, *86*, 370–384.
2. Xian, G.; Crane, M. An analysis of urban thermal characteristics and associated land cover in Tampa Bay and Las Vegas using Landsat satellite data. *Remote Sens. Environ.* **2006**, *104*, 147–156.
3. World's population increasingly urban with more than half living in urban areas | UN DESA | United Nations Department of Economic and Social Affairs.

4. Dihkan, M.; Karsli, F.; Guneroglu, A.; Guneroglu, N. Evaluation of surface urban heat island (SUHI) effect on coastal zone: The case of Istanbul Megacity. *Ocean Coast. Manag.*

5. Streutker, D. R. A remote sensing study of the urban heat island of Houston, Texas. *Int. J. Remote Sens.* **2002**, *23*, 2595–2608.

6. Imhoff, M. L.; Zhang, P.; Wolfe, R. E.; Bounoua, L. Remote sensing of the urban heat island effect across biomes in the continental USA. *Remote Sens. Environ.* **2010**, *114*, 504–513.

7. Ogashawara, I.; Bastos, V. da S. B. A Quantitative Approach for Analyzing the Relationship between Urban Heat Islands and Land Cover. *Remote Sens.* **2012**, *4*, 3596–3618.

8. Liu, K.; Su, H.; Zhang, L.; Yang, H.; Zhang, R.; Li, X. Analysis of the Urban Heat Island Effect in Shijiazhuang, China Using Satellite and Airborne Data. *Remote Sens.* **2015**, *7*, 4804–4833.

9. Fabrizi, R.; Bonafoni, S.; Biondi, R. Satellite and Ground-Based Sensors for the Urban Heat Island Analysis in the City of Rome. *Remote Sens.* **2010**, *2*, 1400–1415.

10. Landsat 8 http://landsat.usgs.gov/landsat8.php (accessed May 20, 2015).

11. Actionbioscience | Urban Heat Islands: Hotter Cities http://www.actionbioscience.org/environment/voogt.html (accessed May 20, 2015).

12. Xiong, Y.; Huang, S.; Chen, F.; Ye, H.; Wang, C.; Zhu, C. The Impacts of Rapid Urbanization on the Thermal Environment: A Remote Sensing Study of Guangzhou, South China. *Remote Sens.* **2012**, *4*, 2033–2056.

13. Chen, X.-L.; Zhao, H.-M.; Li, P.-X.; Yin, Z.-Y. Remote sensing image-based analysis of the relationship between urban heat island and land use/cover changes. *Remote Sens. Environ.* **2006**, *104*, 133–146.

14. Kriegler, F. J.; Malila, W. A.; Nalepka, R. F.; Richardson, W. Preprocessing transformations and their effects on multispectral recognition. In *Remote Sensing of Environment, VI*; 1969; Vol. 1, p. 97.

15. Huete, A. R. A soil-adjusted vegetation index (SAVI). *Remote Sens. Environ.* **1988**, *25*, 295–309.

16. Gao, B. NDWI—A normalized difference water index for remote sensing of vegetation liquid water from space. *Remote Sens. Environ.* **1996**, *58*, 257–266.

17. Zhao, H.; Chen, X. Use of normalized difference bareness index in quickly mapping bare areas from TM/ETM+. In *Geoscience and Remote Sensing Symposium, 2005. IGARSS '05. Proceedings. 2005 IEEE International*; 2005; Vol. 3, pp. 1666–1668.

18. Zha, Y.; Gao, J.; Ni, S. Use of normalized difference built-up index in automatically mapping urban areas from TM imagery. *Int. J. Remote Sens.* **2003**, *24*, 583–594.

19. Xu, H. Modification of normalised difference water index (NDWI) to enhance open water features in remotely sensed imagery. *Int. J. Remote Sens.* **2006**, *27*, 3025–3033.

20. Kawamura, M.; Jayamana, S.; Tsujiko, Y. Relation between social and environmental conditions in Colombo Sri Lanka and the urban index estimated by satellite remote sensing data. *Int Arch Photogramm Remote Sens* **1996**, *31*, 321–326.

21. Xu, H. A new index for delineating built-up land features in satellite imagery. *Int. J. Remote Sens.* **2008**, *29*, 4269–4276.

22. As-syakur Abd Rahman; Adnyana, I. W. S.; Arthana, I. W.; Nuarsa, I. W. Enhanced Built-Up and Bareness Index (EBBI) for Mapping Built-Up and Bare Land in an Urban Area. *Remote Sens.* **2012**, *4*, 2957–2970.

23. Baig, M. H. A.; Zhang, L.; Shuai, T.; Tong, Q. Derivation of a tasselled cap transformation based on Landsat 8 at-satellite reflectance. *Remote Sens. Lett.* **2014**, *5*, 423–431.
24. Drucker, H.; Burges, C. J.; Kaufman, L.; Smola, A.; Vapnik, V. Support vector regression machines. *Adv. Neural Inf. Process. Syst.* **1997**, *9*, 155–161.
25. Using the USGS Landsat 8 Product http://landsat.usgs.gov/Landsat8_Using_Product.php (accessed May 20, 2015).
26. Jimenez-Munoz, J. C.; Sobrino, J. A.; Skokovic, D.; Mattar, C.; Cristobal, J. Land Surface Temperature Retrieval Methods From Landsat-8 Thermal Infrared Sensor Data. *IEEE Geosci. Remote Sens. Lett.* **2014**, *11*, 1840–1843.
27. MOD11A2 | LP DAAC :: NASA Land Data Products and Services https://lpdaac.usgs.gov/products/modis_products_table/mod11a2 (accessed May 22, 2015).
28. Moser, G.; Serpico, S. B. Automatic Parameter Optimization for Support Vector Regression for Land and Sea Surface Temperature Estimation From Remote Sensing Data. *IEEE Trans. Geosci. Remote Sens.* **2009**, *47*, 909–921.
29. Durbha, S. S.; King, R. L.; Younan, N. H. Support vector machines regression for retrieval of leaf area index from multiangle imaging spectroradiometer. *Remote Sens. Environ.* **2007**, *107*, 348–361.
30. Smola, A. J.; Schölkopf, B. A tutorial on support vector regression. *Stat. Comput.* **2004**, *14*, 199–222.
31. Cherkassky, V.; Ma, Y. Practical selection of SVM parameters and noise estimation for SVM regression. **2004**, *17*, 113–126.